Journal of Nano- and Electronic Physics
Vol. **12** No 2, 02029(4pp) (2020)

Журнал нано- та електронної фізики
Том **12** № 2, 02029(4cc) (2020)

Resistive Switching Characteristics of Electrochemically Anodized Sub-stoichiometric Ti_6O Phase

Kiran A. Nirmal[1], Shirish T. Killedar[1], Trishala R. Desai[1], Kishorkumar V. Khot[1], Rajanish K. Kamat[2], Tukaram D. Dongale[1], Deok-kee Kim[3,*]

[1] *Computational Electronics and Nanoscience Research Laboratory, School of Nanoscience and Biotechnology, Shivaji University, Kolhapur 416004, India*
[2] *Department of Electronics, Shivaji University, Kolhapur 416004, India*
[3] *Department of Electrical Engineering, Sejong University, 209 Neungdong-ro, Gwangjin-gu, Seoul 05006, Korea*

(Received 15 February 2020; revised manuscript received 15 April 2020; published online25 April 2020)

We have developed Ti_6O thin film using the electrochemical anodization approach for resistive switching (RS) application. The effect of anodization time (1 h, 2 h and 3 h) on the RS/memristive properties was investigated. The structural analysis was carried out by using the XRD technique, which reveals that the formation of the sub-stoichiometric Ti_6O phase. The scanning electron microscopy image reveals that the thin film has compact and porous surface morphology. The electrical results clearly show bipolar RS in Al/Ti_6O/Ti device. The boost in the RS properties was achieved by increasing the anodization time. The basic memristive properties were calculated using experimental *I-V* data. The Schottky, Hopping and Ohmic charge transport mechanisms contribute to the conduction, whereas the filamentary effect controls the RS process of the Al/Ti_6O/Ti memristive devices.

Keywords: Ti_6O, Electrochemical anodization, Resistive switching, Memristive device.

DOI: 10.21272/jnep.12(2).02029 PACS numbers: 85.90. + h, 68.55. − a, 68.60. − p

1. INTRODUCTION

In recent years, many efforts have been emphasized to replace current flash memory technology. Among many prospective candidates, the resistive switching (RS) based memory, or 'memristor/memristive device,' has become an effective solution for the future nonvolatile memory [1]. Engineering of active switching layer, metal/switching layer interface and biasing conditions can control the resistance state of the memristive device [2]. Therefore, the technological benchmark feature (for memory) could be easily achieved in the near future [3]. Furthermore, the nonlinear memory switching properties of the memristive device can be exploited for the evolution of new nonlinear circuits for a range of applications [4]. In addition to this, the memristive device is finding application in the non-volatile memory, computer logic, and brain-inspired computing [5]. As far as an active switching layer is concerned, lots of new materials have been explored. Among them, transition metallic oxides (TMOs) are used preferentially in memory devices due to their switching stability, easy fabrication technique, low cost and reliability [6].

The titanium oxide (TiO_2) is a promising material for memristive device development [7]. TiO_2 stoichiometry can be obtained by anodizing techniques, basically consists of TiO_2 as well as non-stoichiometric phases ($Ti_{1+x}O_{2-y}$) and sub-stoichiometric phases (Ti_2O_3, TiO, Ti_2O, Ti_6O) [8]. The zero-dimensional electrides such as Ti-rich Ti-O compounds consist of extra electrons which can be useful to improve the conductivity of the end device. Sometimes, the excess electrons are work as an anion; therefore, one can get the excellent RS property from these devices [9]. There are various techniques available for the synthesis of TiO_2 such as sol-gel route, template-assisted methods, hydro/solvothermal approach, and electrochemical deposition [10]. The electrochemical anodization is an efficient and cost-effective way to synthesis the good quality TiO_2 thin films [11].

Here, we report the fabrication of Ti_6O thin films by electrochemical anodization and demonstrated the memristive switching properties of the same. The main advantage of this method is to cultivate good quality porous nanotube arrays. In addition to this, we can easily control the diameter and length of nanotube by merely adjusting the reaction parameters. The electrochemical anodization is an inexpensive, simple, and controlled method to fabricate the stoichiometric and non-stoichiometric phases of TiO_2. The resistive/memristive switching and conduction mechanisms of the Ti_6O thin films are also reported.

2. EXPERIMENTAL DETAILS

2.1. Materials and Methodology

Electrochemical anodization of titanium (Ti) foil (99.7 %, 0.25 mm, Sigma-Aldrich) was carried out by using a high-voltage potentiostat (APLAB, regulated DC power supply) in an electrochemical cell with two-electrode configuration, as represented in Fig. 1a. In this protocol, the conducting electrode (Ti foil) undergoing the anodization was connected to the power supply and dipped into the electrolyte solution, serve as an anode. Whereas platinum wire performed the role of the counter electrode. Initially, Ti foils were polished and sonicated separately in acetone, iso-propanol and ethanol. Finally, Ti foils were rinsed with de-ionized (DI) water and dried for 15 min in a hot air oven at 60 °C. Mixture solution of ethylene glycol (Thomas baker,

* deokkeekim@sejong.ac.kr

Mumbai, India) and polyethylene glycol (Thomas baker, Mumbai, India) with a ratio of 4:1 (v/v) containing 0.25 wt. % NH_4F (Thomas baker, Mumbai, India) and 0.75 wt. % DI water were used for Ti metal anodization to form a thin film. Anodization of titanium foil was carried out at 60 V for 1 h, 2 h and 3 h to prepare Ti_6O thin films. Anodized films were rinsed with DI water and further to annealed at 450 °C for 1 h.

2.2. Possible Mechanism of the Anodization

When metals are subjected to a sufficiently high anodic potential, an oxidation reaction $M \rightarrow Mn^+ + ne^-$ was initiated. In this case, three possible reactions can happen: 1) The Mn^+ ions were solvatized in the electrolyte; 2) the Mn^+ ions react with O_2. Therefore, a compact oxide layer was form; 3) struggle between solvatization and oxide formation could lead to the formation of porous oxide [12].

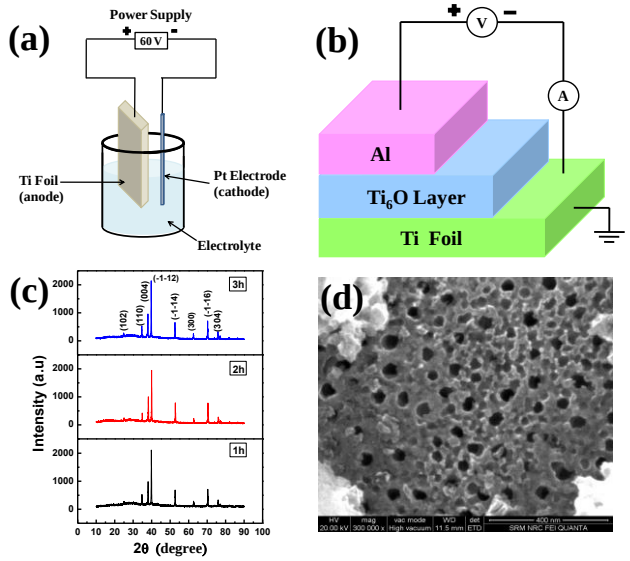

Fig. 1 – Schematic of the electrochemical cell for anodization of Ti foil (a); device structure Al/Ti6O/Ti (b); XRD of Ti_6O thin films at different deposition time (c); SEM image of anodized Ti foil (d)

3. RESULTS AND DISCUSSION

Fig. 1c represents the XRD (D2 phase) pattern of the Ti_6O thin films, anodized at various anodization time (1 h, 2 h and 3 h). XRD results suggested that the prepared Ti_6O thin films were nanocrystalline and show hexagonal crystal properties (JCPDS No. 01-072-1807) [13]. The intensity of the diffracted peaks increases as the deposition time increases. The – 1-12 plane was observed as a most intense peak from the XRD results. The other low intense planes such as 102, 110, 004, – 1-14, 300, – 1-16 and 304 were associated with 27.49°,34.95°, 37.93°, 52.53°, 62.68°, 69.86°, and 75.66° diffraction peaks, respectively. The average crystallite size (D) was calculated by using Scherrer's relation [14] and found to be 9.14, 9.27 and 8.50 nm for 1, 2, and 3 h deposited Ti_6O thin films, respectively. The lattice parameters of developed Ti_6O thin films were $a = b = 5.1300$ Å and $c = 9.4800$ Å. Fig. 1d represents the SEM (Quanta) micrograph of 3 h deposited Ti_6O thin film. The SEM image suggested that the compact and porous surface morphology was created during the anodization of Ti foil. Furthermore, the porous surface morphology has uniformly covered the sample and the average pore diameter was found to be ~ 45 nm. This kind of porous structure is responsible to improve the surface area and conductivity of the sample. Furthermore, it also helps to contribute the better charge transport properties.

Electrical measurements (ArC ONE) were carried out by grounding the Ti substrate and applying a positive bias to the top Al electrode. The memristive behavior of the fabricated devices was characterized by sweeping the bias voltage from 0 V to 4 V, 4 V to 0 V, 0 V to – 4 V and – 4 V to 0 V and the corresponding current was recorded. Fig. 2 reveals the *I-V* properties of the Al/Ti_6O/Ti devices, deposited at different at anodization time such as 1 h, 2 h and 3 h. Arrows designate the switching direction of the Al/Ti_6O/Ti device. In the present case, Al/Ti_6O/Ti devices are considered as memristive device due to the observed hysteresis loop during *I-V* measurements [15]. Furthermore, bipolar RS is observed in all developed devices. The shifting of the resistance state of the device from HRS to LRS was observed at + 4 V (SET voltage).

On the other hand, – 4 V (RESET voltage) switching voltage point shows another shifting location i.e. LRS to HRS transition. Therefore, the Al/Ti_6O/Ti-based device exhibits bipolar RS characteristics. It is observed that the positive and negative biased loops are asymmetrical and demonstrating the rectifying property. The origin of the asymmetry and rectifying property is due to the interface effects [16]. The RS property of the Al/Ti_6O/Ti devices was boosted proportionally to the anodization time. In particular, a 3 h deposited active layer shows excellent RS property than other devices.

In order to demonstrate the memristive effect in the Al/Ti_6O/Ti devices, we have calculated essential memristive characteristics from the experimental *I-V* data. The time-domain current characteristic is shown in Fig 3a and the inset represents the time domain voltage characteristics.

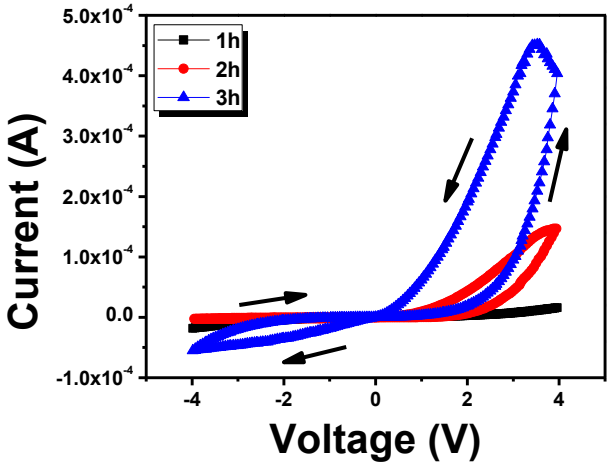

2 – Anodization time-dependent *I-V* characteristics of Al/Ti_6O/Ti devices

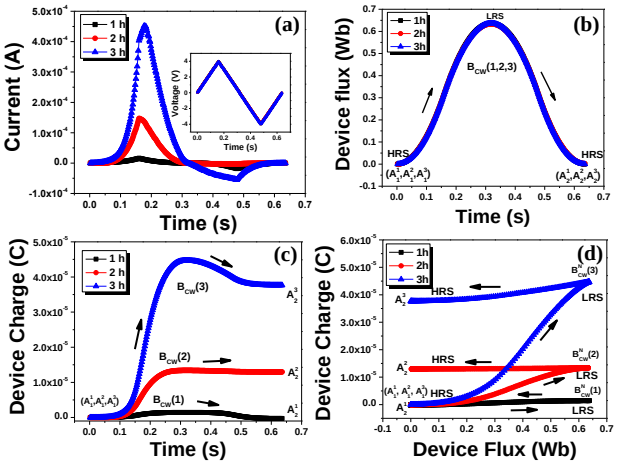

Fig. 3 – Time-domain current (inset: time-domain voltage) (a), flux (b), charge (c) and charge-flux (d) characteristics of the Al/Ti_6O/Ti memristive devices

The time-domain current shows typical rectifying behavior i.e. maximum current at positive bias and minimum current at negative bias. Increment in peak current was observed with an enhancement of deposition time from 1 h to 3 h. Fig. 3b shows time-domain flux property in which all data are overlaps on each other due to the symmetric voltage stimulus. The initial period (A_1^1, A_1^2 and A_1^3), half period (B_{CW} 1, 2, and 3), final period (A_2^1, A_2^2, and A_2^3) and turning point (B_{CW}^N 1, 2, and 3) indicate RS state of Al/Ti_6O/Ti memristive devices. The arrow represents the switching direction form HRS to LRS and backs to HRS. Fig. 3c represents the time domain charge characteristic of the Al/Ti_6O/Ti thin-film devices. The results suggested the asymmetric nature of the time domain charge properties of the Al/Ti_6O/Ti memristive devices. This kind of asymmetry in the time domain charge characteristic is attributed due to the irregular RS loops. The results further confirm that the value of charge tends to rise with deposition time. Furthermore, the values of the initial period for each device are found to the same while values of half and final period are found to differ due to the different *I-V* nature of each device. The charge-flux properties of Al/Ti_6O/Ti memristive devices are shown in Fig. 3d. Similar to the time domain charge, the charge-flux property of Al/Ti_6O/Ti memristive devices is asymmetric. Furthermore, A_1^x, B_{CW}, A_2^x, and B_{CW}^N are found to depend on the deposition time of the Ti_6O active switching layer. In this case, the RS state values are found to be increases as the deposition time of the Ti_6O active switching layer increases. It is relevant to note that double valued charge-flux characteristics are observed for each Al/Ti_6O/Ti thin-film device, suggesting the ascendency of the memristive nature rather than ideal memristor behavior [17].

For the understanding of the RS process of the Al/Ti_6O/Ti memristive devices, the optimized 3 h deposited device was used as a representative device. For this, *I-V* data was divided into various sections and current transport models were fitted to *I-V* data. Figs. 4a-f show the conduction model fitting results of Al/Ti_6O/Ti memristive devices. In this case, positive biased low voltage (0 V to + 1 V), high voltage (+ 1 V to + 4 V) and entire (0 V to + 4 V) regions were created, as shown in Figs. 4a-c, respectively. On a similar line negative biased entire (0 V to – 4 V), high voltage (– 1 V to – 4 V), and low voltage (0 V to – 1 V) regions were created, as shown in Figs. 4d-f, respectively. In the present case, three different types of conduction models were well fitted to *I-V* data. For instance, the HRS *I-V* data i.e. positive and negative biased low voltage regions were fitted to the Schottky model whereas; high voltage regions were fitted to the Hopping conduction model. The LRS *I-V* data (entire voltage region) of both bias conditions were well fitted to the Ohmic conduction model. All adjacent R^2 values were higher than 0.90, indicated that the experimental *I-V* data has close resemblance with fitted models.

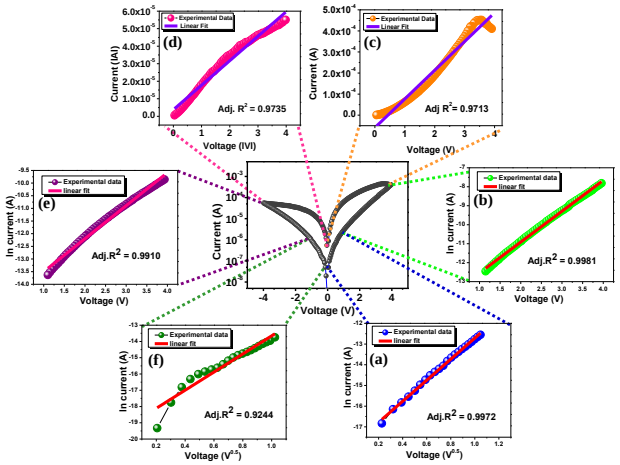

Fig. 4 – Conduction mechanism of Al/Ti_6O/Ti memristive device. The model-fitting results of the positively biased low (a), high (b), entire voltage regions (c), negatively biased entire (d), high (e) and low (f) voltage regions

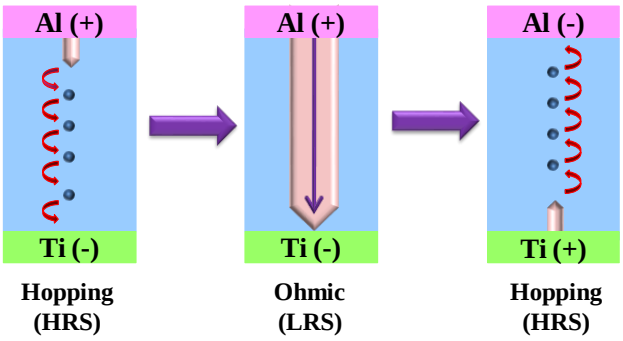

Fig. 5 – Probable filamentary RS mechanism of the Al/Ti_6O/Ti memristive device with the assistant of interfacial effects

Based on the fitting results and experimentally obtained *I-V* nature, we proposed a probable filamentary RS mechanism with the assistant of interfacial effects, as shown in Fig. 5. During positive biased low voltage, electrons from the top electrode were unable to move in the switching layer due to the presence of Schottky contact at the Al/Ti_6O interface. Because of this contact, a small amount of current was passed through the device and the device shows the HRS. When positive bias was increased further, the discrete metal precipitates and electrons start to hop from one trap to another trap, results in the formation of discontinuous conductive filament [18]. At the SET voltage, the numbers

of metal ions accumulate and form a complete conductive filament, which corresponds to the LRS of the device. As the polarity of the signal changes, the device undergoes in the HRS due to the Hopping and Schottky conduction mechanisms. The cyclic change in the resistance states, from HRS to LRS and vice versa due to the external bias, the Al/Ti_6O/Ti memristive devices show the bipolar RS effect.

4. CONCLUSIONS

In conclusion, we have employed the electrochemical anodization method to fabricate the Ti_6O RS layer. The XRD analysis reveals that the formation of the substoichiometric Ti_6O phase. The SEM image of the optimized sample suggested that the formation of a compact and porous thin film with an average pore diameter was found to be ~ 45 nm. The developed Al/Ti_6O/Ti device shows the anodization time (1 h, 2 h and 3 h) dependent bipolar RS/memristive characteristics. The asymmetric charge and two-valued charge-flux properties suggested the memristive nature of the Al/Ti_6O/Ti device. The conduction in the device was due to the Schottky, Hopping and Ohmic charge transport mechanisms whereas, forming and breaking of filament control the bipolar RS process of the Al/Ti_6O/Ti memristive devices.

ACKNOWLEDGEMENTS

This study was supported by the Basic research program (2016R1D1A1B01009537) through the National Research Foundation (NRF) of Korea and by the MOTIE (Ministry of Trade, Industry and Energy (10080581) and KSRC (Korea Semiconductor Research Consortium) support program for the development of the future semiconductor device.

REFERENCES

1. K. Nagashima, T. Yanagida, K. Oka, M. Kanai, A. Klamchuen, J.S. Kim, B.H. Park, T. Kawai, *Nano Lett.* **11**, 2114 (2011).
2. R. Muenstermann, T. Menke, R. Dittmann, R. Waser, *Adv. Mater.* **22**, 4819 (2010).
3. S. Stathopoulos, A. Khiat, A. Serb, T. Prodromakis, *IEEE Int. Symp. Circ. Sys. (ISCAS)* 1 (2016).
4. J. Sun, X. Zhao, J. Fang, Y. Wang, *Nonlinear Dyn.* **94**, 2879 (2018).
5. K.K. Pawar, D.V. Desai, S.M. Bodake, H.S. Patil, S.M. More, A.S. Nimbalkar, S.S. Mali, C.K. Hong, S. Kim, P.S. Patil, T.D. Dongale, *J. Phys. D: Appl. Phys.* **52**, 175306 (2019).
6. T.D. Dongale, K.V. Khot, S.V. Mohite, S.S. Khandagale, S.S. Shinde, V.L. Patil, S.A. Vanalkar, A.V. Moholkar, K.Y. Rajpure, P.N. Bhosale, P.S. Patil, *J. Nano Electron. Phys.* **8**, 04030 (2016).
7. A.C. Khot, N.D. Desai, K.V. Khot, M.M. Salunkhe, M.A. Chougule, T.M. Bhave, R.K. Kamat, K.P. Musselman, T.D. Dongale, *Mater. Design* **151**, 37 (2018).
8. M.V. Diamanti, S. Codeluppi, A. Cordioli, M.P. Pedeferri, *J. Exp. Nanosci.* **4**, 365 (2009).
9. X. Zhong, M. Xu, L. Yang, X. Qu, L. Yang, M. Zhang, H. Liu, Y. Ma, *NPJ Comput. Mater.* **4**, 70 (2018).
10. M.M. Byranvand, N.A. Kharat, L. Fatholahi, M.Z. Beiranvand, *J. Nano Struct.* **3**, 1 (2013).
11. G. Liu, K. Du, and K. Wang, *Appl. Surface Sci.* **388,** 313 (2016).
12. P. Nyamukamba, O. Okoh, H. Mungondori, R. Taziwa, S. Zinya, *Titanium Dioxide: Material for a Sustainable Environment* 151 (London: Intech Open: 2018).
13. J. Krysa, H. Krysova, Z. Hubicka, S. Kment, J. Maixnerand, L. Kavan, *Photochem. Photobio B* **18**, 891 (2019).
14. S. Patil, M. Chougale, T. Rane, S. Khot, A. Patil, O. Bagal, S. Jadhav, A. Sheikh, S. Kim, T. Dongale, *Electronics* **7**, 445 (2018).
15. D.B. Strukov, G.S. Snider, D.R. Stewart, R.S. Williams, *Nature* **453**, 80 (2008).
16. Y. Tian, C. Guo, S. Guo, T. Yu, Q. Liu, *Nano Res.* **7**, 953 (2014).
17. V.S. Dongle, A.A. Dongare, N.B. Mullani, P.S. Pawar, P.B. Patil, J. Heo, T.J. Parkand, T.D. Dongale, *J. Mater. Sci.-Mater. Ele.* **29**, 18733 (2018).
18. E.W. Lim, R. Ismail, *Electronics* **4**, 586 (2015).